Flood Detection Using GRACE Terrestrial Water Storage and Extreme Precipitation

Jianxin Zhang [1,2], Kai Liu [1], Ming Wang [1]

[1] School of National Safety and Emergency Management, Beijing Normal University, 100875 Beijing, China
[2] School of Systems Science, Beijing Normal University, 100875 Beijing, China

Correspondence to: Kai Liu (liukai@bnu.edu.cn)

Abstract. A complete global flood event record helps researchers analyse the distribution law of global floods and better formulate and manage disaster prevention and reduction policies. This study used GRACE terrestrial water storage and precipitation data combined with high-frequency filtering, anomaly detection and flood potential index methods to successfully extract historical flood days globally between Apr. 1st, 2002, and Aug. 31st, 2016, and further compared and validated the results with Dartmouth Flood Observatory (DFO) data, Global Runoff Data Centre (GRDC) discharge data, news reports and social media data. The results showed that GRACE-based flood days could cover 81% of the flood events in the DFO database, 87% of flood events extracted by MODIS and supplement many additional flood events not recorded by the DFO. Moreover, the probability of detection greater than or equal to 0.5 reached 62% among 261 river basins compared to flood events derived from the GRDC discharge data. These detection capabilities and detection results are both good. We finally provided flood day products with 1° spatial resolution covering the range of 60°S—60°N from Apr. 1st, 2002, to Aug. 31st, 2016. This research provides a data foundation for the mechanistic analysis and attribution of global flood events.

1 Introduction

Flood disasters threaten the lives of millions of people around the world every year, causing more economic losses than any other natural disaster. An increasing number of extreme weather events are occurring frequently under global climate change (Schinko et al., 2017). The latest research on global flood disasters shows that the proportion of the population at risk from floods is increasing each year (Tellman et al., 2021).

Existing global flood data mainly include historical data records, hydrological model simulations and remote sensing observations. Historical data records include those of the Dartmouth Flood Observatory (DFO) (Brakenridge, 2022), international disasters database (EM-Dat) (Em-Dat, 2014), Munich Re's NatCatSERVICE (natcatservice.munichre.com), and Sigma (Re, 2022). The DFO database mainly records large-scale flood events from news reports, government, instrumental, and remote sensing source. This database records not only the country, latitude, approximate scope and start and end time of each event but also the cause and severity level of the event. There have been approximately 4,700 major flood events since 1985. EM-Dat contains basic core data on the occurrence and impact of more than 22,000 large-scale disasters in the world from 1900 to the present. This database is compiled from a variety of sources, including UN agencies, nongovernmental organizations, insurance companies, research institutes and news organizations. NatCatSERVICE is a natural hazard-based disaster loss database with up to 28,000 entries owned by Munich Re's company. Sigma is also a global disaster database comprising anthropogenic and natural catastrophe losses since 1970. In addition to recording basic disaster information, this database also includes the total and insured losses. Flood data are also derived from global hydrological models. For example, the University of Maryland's Global Flood Monitoring System (GFMS) takes real-time integrated precipitation information (Tropical Rainfall Measuring Mission (TRMM) and Global Precipitation Measurement (GPM)) as inputs in a quasi-global (50°N - 50°S) hydrological runoff and routing model to run 1/8° gridded data. Surface water storage statistics are used to derive flood thresholds for each grid location, and the depth above the corresponding threshold is calculated as the flood intensity (Wu et al., 2014; Wu et al., 2012a; Wu et al., 2012b; Wu et al., 2011). Another example is the Floods.Global system

(http://floods.global) database, in which GPM Integrated Multi-satellite Retrievals for GPM (IMERG) precipitation data are used to estimate future 72-hour flows, with coverage from 60°N to 60°S and a resolution of 0.1 degrees. With the development of remote sensing satellite products in the 1980s, a cost-effective flood-monitoring method is developed. As long as there are historical areas over which satellites have passed and imaged, there are opportunities to observe flood events; these methods are more realistic and effective than flood models in characterizing actual observed flood areas. Commonly used remote sensing data include optical remote sensing images and microwave remote sensing images, among which microwave remote sensing technologies, especially the commonly applied synthetic aperture radar (SAR), are used. Rättich et al. (2020) developed an automatic procedure to evaluate flood durations and uncertainties using multiple satellites, including Sentinel-1, Sentinel-2, Landsat-8 and TerraSAR-X. The method was successfully demonstrated on the 2019 flood in Sofala, Mozambique and on the 2017 flood in Bihar, India. Tellman et al. (2021) used 250-m-resolution Moderate-resolution Imaging Spectroradiometer (MODIS) data to extract the inundation extents of a total of 913 global flood events from 2000 to 2018, thus providing data support for vulnerability assessments and flood model improvements. Tong et al. (2018) used both Landsat 8 optical imagery and COSMO-SkyMed radar imagery combined with a support vector machine and the active contour without edges model to perform flood monitoring. The results showed high accuracies of 97.46% for optical imagery and 93.70% for radar imagery.

However, there are some limitations in current databases. NatCatSERVICE, EM-Dat and Sigma provide data only at the country level. The NatCatSERVICE database covers most large flood events around the world but only a few small flood events in developing countries due to restricted connectivity (De Bruijn et al., 2019). Although there are approximate map locations available in the Sigma and NatCatSERVICE databases, specific location names are not publicly available (Moriyama et al., 2018). Moreover, both the NatCatSERVICE and Sigma databases are developed by reinsurance companies, and the accessibility of the information in these databases is limited (Moriyama et al., 2018; Kron et al., 2012; Huggel et al., 2015). The EM-Dat database records only the numbers of flood events in different countries without corresponding spatial location information. Although DFO records the start and end times and the approximate spatial locations of flood events, the duration is sometimes long (more than one or two months), and the spatial locations are only roughly delineated according to news reports. Tellman et al. (2021) extracted flood extents and analysed the population exposure of 913 large-scale flood events from 2000 to 2018 based on MODIS daily data with a resolution of 250 metres, thus finely delineating the spatial inundation extent. During this period, there were more than 3,000 flood events recorded in the DFO database, while the number of MODIS-derived floods was less than 30% of that recorded by DFO. The numbers of flood events recorded in China, Russia and Canada are obviously lacking. Moreover, flood detection methods based on remote sensing data are mainly aimed at specific flood events in small areas and are influenced by the number of revisit cycles at the same location (especially for SAR images) and bad weather (especially for optical images) (Kussul et al., 2011; Hostache et al., 2018; Manavalan, 2017). The spectral information of optical remote sensing image is influenced by clouds, which affects the quantitative inversion of flood extent based on remote sensing. SAR image lacks revisits of the same location for flood change detection. These shortcomings affected the flood extraction accuracy. There is a need to fill in the missing flood events with a new observational dataset.

Another remote sensing technique based on gravity satellites, the Gravity Recovery and Climate Experiment Satellite (GRACE), has also been successfully used to detect flood events. Reager and Famiglietti (2009) first proposed the terrestrial water storage capacity and flood potential, creating a precedent for GRACE to assess large-scale flood events. This method was subsequently improved and applied to different river basins. Molodtsova et al. (2016) found an agreement between the flood potential index derived from GRACE and recorded floods by using multiyear flood observation data from 2003 to 2012 by the US Geological Survey and DFO. Gupta and Dhanya (2020) proved that GRACE terrestrial water storage (TWS) and the flood potential index had the capability to assess hydrological extreme events over heterogeneous regions with the occurrences of high- and long-duration floods. They suggested that flood potential index can be useful for flood monitoring when discharge data are rarely available. With the continuous progress of the global GRACE-only gravitational field solution,

GRACE daily data products have also been effectively developed and applied (Kvas et al., 2019; Mayer-Gürr et al., 2018). Gouweleeuw et al. (2018) used a daily solution based on GRACE TWS and daily river runoff data to assess major flood events in the Ganges-Brahmaputra Delta and confirmed the method's potential for gravity-based large-scale flood monitoring. Xiong et al. (2022) used daily downscaled GRACE data to detect short-duration and high-intensity floods. They found that there was a strong correlation between the high-frequency components of GRACE TWS and runoff.

In this study, we focus on extracting global historical flood events based on daily GRACE and precipitation data. Apart from being affected by battery management in some months, GRACE's gravity measurements cover most months and are not affected by varying kinds of weather conditions. This study mainly extracted all flood days in the historical time series caused by extreme precipitation, regardless of whether the flood event caused severe damage. Finally, we provided global flood days with a resolution of 1° during the period from Apr. 1st, 2002 to Aug. 31st, 2016. These data replenish the missing flood events in the historical record and provide a new and complete flood dataset, thus providing a sufficient data foundation for research on the inducement of global floods.

2 Data

2.1 Daily GRACE TWS

The GRACE constellation is a pair of twin satellites that can measure changes in Earth's gravitational field. There is a precise radar rangefinder between the two satellites. When Earth's gravitational field changes slightly, it can be detected by either of the two satellites. The distance signal between the two satellites is amplified to measure the state change at the current moment relative to the previous moment (Cazenave and Chen, 2010). The short-term gravitational field changes of Earth are mainly caused by changes in terrestrial water storage, atmospheric water vapour, ocean tides, etc. When these signals are deducted, the change in the entire terrestrial water storage can be inverted (Wahr et al., 1998). The daily GRACE data selected in this study come from daily solutions obtained using Kalman smoothing by Mayer-Gürr et al of Graz University of Technology based on ITSG-Grace2018 gravity field model. The ITSG-Grace2018 gravity field model, which offers unconstrained monthly and Kalman-smoothed daily solutions, is the most recent GRACE-only gravity field model computed in Graz (Mayer-Gürr et al., 2018). The time period spans from Apr. 1st, 2002, to Aug. 31st, 2016, the resolution is 1° and the unit is "m". A third-order autoregressive (AR) model was used to stabilize the daily solution. A set of spherical harmonic coefficients for the various degrees (n=2…40) was estimated. When GRACE data were not available for a specific day, daily solutions were delivered through an adjustment process (Bergmann-Wolf et al., 2015; Dill et al., 2008). This processed data can be obtained from the website: https://www.tugraz.at/institute/ifg/downloads/gravity-field-models/itsg-grace2018/.

2.2 Precipitation

This study used Global Precipitation Measurement (GPM) data to calculate extreme precipitation. GPM is an international satellite mission launched by the National Aeronautics and Space Administration (NASA) and Japan Aerospace Exploration Agency (JAXA). It is the next-generation and high-quality global rain and snow satellite observation network after the TRMM. GPM provides important data foundation for scientific researchers to understand the Earth's water resources and energy cycles and improve their ability to predict extreme events (Huffman et al., 2015). The resolution of these data is 0.1°, with the unit of "mm", mainly covering the range of 60°S—60°N, and both north-south latitudes of 60—90° have partial coverage. This study selects the IMERG Final Run product, which uses global microwave precipitation data, infrared data, precipitation station data and other potential precipitation indicators to cross-calibrate, fuse and interpolate TRMM and GPM data at refined temporal and spatial scales. It is an officially recommended product and can be obtained from the following website: https://gpm.nasa.gov/data/directory. To remain consistent with the GRACE resolution and maintain extreme precipitation

signals, we take the maximum values of the precipitation covered by each 1° GRACE grid to further calculate the flood potential index and the number of extreme precipitation days.

2.3 Flood events from Dartmouth Flood Observatory

The DFO dataset records large flood events from various news reports, government, instrumental, and remote sensing source. It contains the start and end times of each flood, the country where it occurred, the approximate flood extent, the cause of the flood and the degree of damage. It is a rare and useful product for studying global historical floods. This data product has been widely used in flood hazard science research (Tellman et al., 2021; Hagen et al., 2010; Winsemius et al., 2013; Idowu and Zhou, 2019). This study focuses on precipitation-induced floods. A total of 2380 flood events in the 60°S—60°N range were caused by heavy precipitation between Apr. 1st, 2002 and Aug. 31st, 2016. This product was primarily used to validate the flood data extracted in this study and can be obtained from https://floodobservatory.colorado.edu/Archives/index.html.

2.4 MODIS-derived Flood Inundation Data

The flood inundation extent data used in this study come from a total of 807 flood events extracted based on MODIS data by Tellman et al. (2021) in the 60°S—60°N region from Apr. 1st, 2002 to Aug. 31st, 2016. This product was produced based on atmospherically corrected Terra (MOD09GA/GQ) and Aqua (MYD09GA/GQ) MODIS images. Then the authors used threshold analysis methods (including standard and Otsu-optimized thresholds methods) and slope constraints (slopes greater than 5° were masked out) to extract inundations at a 250-m spatial resolution according to the flood events recorded by the DFO (Tellman et al., 2021). The MODIS-based floods were compared and verified for coincidence with the 30-m-resolution inundation data derived from Landsat 5, 7 and 8 imageries, and flood map quality control analysis was also performed. This product relies on the Google Earth Engine platform (Gorelick et al., 2017), which can be obtained from the following site: https://developers.google.com/earth-engine/datasets/catalog/GLOBAL_FLOOD_DB_MODIS_EVENTS_V1. These data were further refined on the basis of DFO-recorded approximate flood extent and provided reliable spatial inundation dataset for verification in our study.

2.5 GRDC Discharge Data

The Global Runoff Data Centre is an international data centre operating under the auspices of the World Meteorological Organization. It was established in 1988 to support research on global climate change and integrated water resource management. We downloaded the global mean daily discharge data from the https://www.bafg.de/GRDC/EN/Home/homepage_node.html, which additionally contained other attributes like country, longitude, latitude and river name associated with each flood event. The unit of mean daily discharge is m^3/s and the stations with more than 50% missing days in research time period (Apr. 1st, 2002—Aug. 31st, 2016) were excluded to ensure the accuracy. Finally, we obtained 3408 stations from Apr. 1st, 2002—Aug. 31st, 2016 as the validation dataset to verify the GRACE-derived flood days.

3 Methods

Figure 1 shows the technical route of this study. It mainly consists of data preparation, flood days extraction, and result verification. Daily precipitation and daily GRACE TWS data are used for the flood data extraction step, and daily discharge, DFO, MODIS-derived flood inundation and social media data are used for the flood validation step. The flood extraction step is mainly based on high-frequency signals of TWS and the flood potential index to obtain the pre-selected possible flood days; then, extreme precipitation constraints are used to obtain the final flood days. The flood validation includes comparisons with

the DFO-recorded flood extent, MODIS-derived flood inundation, GRDC discharge-derived flood events and significant flood events recorded on social media.

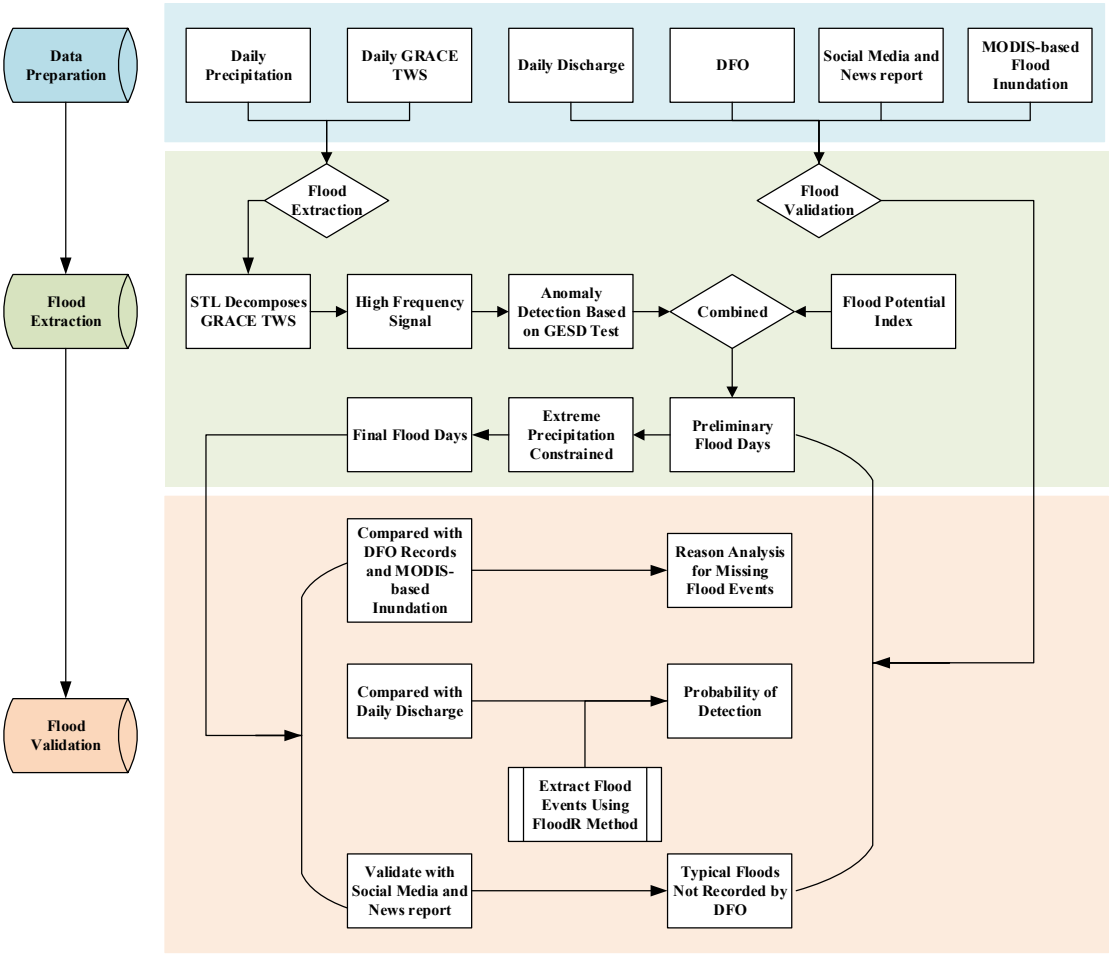

Figure 1 Workflow of the global flood extraction approach based on GRACE and precipitation data.

3.1 Seasonal and Trend decomposition using Loess (STL)

Extreme precipitation has sudden characteristics, and its signals are reflected in the high-frequency signals of GRACE (Xiong et al., 2022; Gouweleeuw et al., 2018). Seasonal and trend decomposition using loess (STL) (Robert et al., 1990) is a filtering process as well as a general and robust time series decomposition and forecasting method used to decompose time series variables into seasonal, trend and remainder components for further forecasting. This process can handle data with any type of seasonality as well as high-frequency signal data. It also allows seasonal components to vary over time and is robust to outliers. In this study, we selected this method as a high-pass filtering tool to process GRACE TWS and obtain high-frequency signals (excluding seasonal and trend components) for subsequent analyses. In this study, the STL function in the R language "stats" package was used to process all grid time series corresponding to the GRACE TWS period (Apr. 1st, 2002—Aug. 31st, 2016). The two main parameters, "t.window" and "s.window", should be specified when using STL. "t.window" is the number of consecutive observations when estimating the trend-cycle and it was set to 31-day window to cover the month and separates daily data according to Gouweleeuw et al. (2018) and Xiong et al. (2022). "s.window" is the number of consecutive years when estimating each value in the seasonal component and it was set to 360 which was determined using a Fourier transform to convert to the frequency domain to obtain the frequency corresponding to the maximum amplitude.

3.2 Anomaly Detection Based On Generalized Extreme Studentized Deviate Test

The generalized extreme Studentized deviate (GESD) test (Rosner, 1983) is a simple and effective statistical method for detecting one or more outliers in univariate data that follow an approximately normal distribution. It has been widely used in the field of hydrological anomaly detection (Saghafian et al., 2014; Clark and Zipper, 2016). GESD test is mainly used in this study to extract possible flood days corresponding to the high-frequency signals. In this study, the method to be selected for extracting flood information from the high-frequency signals should ensure that it was affected by the random error in the high-frequency signal as little as possible and that the flood signals were extracted as much as possible. The method requires only that an upper bound for suspected outliers be specified and determines the number of possible outliers based on hypothesis testing (Rosner, 1983). The basic assumptions of GESD are as follows:

H_0: There are no outliers in the dataset.

H_a: There are at most *r* outliers in the dataset.

The corresponding statistic is calculated as follows:

$$R_i = \frac{max_i |x_i - \bar{x}|}{\sigma} \quad (1)$$

where $\bar{x}$ and σ are the sample mean and standard deviation, respectively. After each iteration in which the largest $|x_i - \bar{x}|$ value is removed, the remaining statistics are calculated, and the above process is repeated until at most *r* outliers are removed. Consistent with the *r* test statistics, the *r* critical values are computed as follows:

$$\lambda_i = \frac{(n-i)t_{p,n-i-1}}{\sqrt{(n-i-1+t^2_{p,n-i-1})(n-i+1)}} \quad i = 1,2,\dots,r \quad (2)$$

$$p = 1 - \frac{\alpha}{2(n-i+1)} \quad (3)$$

where $t_{p,v}$ is the 100p percentage point in a t-distribution with *v* degrees of freedom and α is the significance level. The number of final outliers is then determined by the corresponding maximum *i* value in $R_i > \lambda_i$ (Rosner, 1983).

Considering that the GRACE high-frequency signal contains both random errors and useful signals, we used the GESD test to control the number of outliers so that they were not affected by subjective thresholds. In this study, the "AnomalyDetection" package (https://github.com/twitter/AnomalyDetection) (Aggarwal, 2013; Chandola et al., 2009; Rosner, 1983; Vallis et al., 2014) was used to extract GRACE HPF data. This package not only includes the GESD algorithm but can also specify the direction of detected outliers. The parameter "direction" indicates whether to extract peaks or valleys and "pos" means the extraction of peaks, and "neg" means the extraction of valleys. As we considered extreme weather events caused by heavy precipitation in this study, important information was contained in the peak. The main parameter "direction" was set to the "pos", and the maximum possible number of abnormal days "max_anoms" was set to 0.1 to cover the maximum number of abnormal days among the global time series comprising every grid. We have taken an example in Figure S1 to show the process of extracting possible flood days from high-frequency signals of GRACE TWS using GESD test method as well as the reason for missing some flood events. We have also considered the reliability of the GESD test method in Figure S2.

3.3 Flood Potential Index

We used the probable flood days extracted by flood potential index (FPI) as a complement to the inability to detect flood events with high-frequency signals. The FPI mainly considered rainfall-induced floods and has been widely used to evaluate flood events (Gupta and Dhanya, 2020; Molodtsova et al., 2016; Reager et al., 2014). Its basic assumption is that the regional water storage capacity can be approximated by the maximum value of historical TWS time series. The water storage capacity at the current time can be calculated by subtracting the TWS at the previous time from the maximum value of TWS time-series. The proposal of this method was based on monthly data, but this does not affect the application of GRACE daily data. The detailed descriptions were as follows.

The water storage capacity of the current day can be expressed as the temporal difference between the maximum time-series value and the previous-day value, and the formula is expressed as follows:

$$TWS_{DEF}(t) = TWS_{MAX} - TWS(t-1) \quad (4)$$

where $TWS_{DEF}(t)$ represents the maximum allowable relative water storage change on the current day, TWS_{MAX} represents the maximum value over the entire time series, and $TWS(t-1)$ represents the TWS value of the current day relative to the previous day. A low storage deficit and high precipitation mean a high probability of flooding, i.e., the occurrence of floods should be based on the mismatch between the extreme precipitation level and the increase in water storage:

$$F(t) = P_{day}(t) - TWS_{DEF}(t) \quad (5)$$

where $P_{day}(t)$ represents the daily precipitation and $F(t)$ represents whether the current precipitation matches the water storage capacity. When $F(t) > 0$, flooding may occur. This study uses the flood potential index to supplement possible flood days in case the daily GRACE TWS data have lost useful high-frequency signals due to the interpolation process. We have taken an example in Figure S3 to present flood potential index was able to supplement some flood events not identified by GRACE high-frequency signals.

3.4 Flood Detection Based on GRACE TWS and Precipitation Data

The flood extraction mainly went through pre-selection stage and final selection stage. We first used GRACE HPF data combined with GESD method and flood potential index to preselect the possible flood days pixel by pixel. Next, we further used the number of extreme precipitation days to constrain and obtain the final flood days. This study focuses on flood events caused by heavy precipitation. Considering that floods are caused not only by single-day precipitation but also by cumulative precipitation, we calculated the extreme precipitation days based on the one-day precipitation, 3-day cumulative precipitation and 5-day cumulative precipitation. Regarding extreme precipitation, the most commonly used metric is the percentiles of the precipitation time-series data, including the n-th quantiles of the entire time series data; alternatively, the n-th quantile of wet days (daily precipitation > 1 mm) can be considered (Myhre et al., 2019; Pendergrass, 2018; Shi et al., 2021). In order to present the calculation process more clearly, we randomly selected a spatial grid for detailed processing. Figure S4 showed the intermediate process of flood days extraction. 1) we firstly extracted the high-frequency signal of TWS using the STL method; 2) then we calculated the possible flood days using the GESD method; 3) Next, we use flood potential index to supplement possible flood days in case the daily GRACE TWS data have lost useful high-frequency signals due to the interpolation process. 4) Finally we constrained the pre-selected floods using the extreme precipitation days derived from daily and cumulative precipitation. Based on the principle of extracting as many flood events as possible with as few errors as possible, we choose the 95th quantile of the entire time series as the condition to constrain the flood days extracted from GRACE data. We also provide GRACE-based flood days obtained with the 90th and 99th quantiles of the entire time series data and wet days in supplementary data files.

3.5 Flood Event Extraction Based on Daily Discharge Data

To verify the reliability of the extracted results, this paper used the global discharge data products released by GRDC and the statistics-based automated flood event extraction (FloodR) method to extract possible flood events. FloodR is a statistical-based flood event separation method proposed by Fischer et al. (2021). It can automatically separate flood events using a univariate daily discharge time series, and it integrates expert knowledge tools to manually and quickly validate and correct the separation results. Considering that the fluctuation of daily discharge data is smoother than that of hourly discharge data, FloodR used the moving-window variance to overcome the lower dynamic characteristics of daily discharge. It's basic rules including three points: 1) a flood event is an event that temporarily exceeds the normal discharge, and the start and end of each flood event can be defined; 2) a flood event can be characterized by significantly increased dynamics of discharge; 3)

the sum of the increasing discharges is similar to the sum of the recession of the flood event (Fischer et al., 2021). FloodR can also automatically handle missing data, and perform flood separation in segments according to the missing data and finally merge them. In this paper, the function "eventsep" in FloodR package was used and the parameters was default according to the results of author's practice while the parameter "NA_mode" is based on whether there are missing values in the discharge time series. The results extracted by FloodR include information like the start and end times of each flood, the flood peak date and the flood baseflow, etc., thus providing an important data foundation for verifying the time-series comparison ability of this study.

We use goodness of flood separation (GFS) to evaluate the performance of FloodR method. This indicator explicitly minimizes the number of small runoff events and maximizes the number of flood events with high discharge. This indicator can be used to address the situation of lacking a consistent and true data foundation for evaluate the goodness of flood separation (Fischer et al., 2021).

$$GFS = \left(\frac{Q_{Q>TH_{upper;Flood}}}{Q_{Q>TH_{upper}}}\right) - \max\left(\frac{Q_{Q>TH_{lower;Flood}}}{Q_{Q>TH_{lower}}} - Tol_{lower}, 0\right) \quad (6)$$

Where $Q_{Q>TH_{upper;Flood}}$ is the number of flood days with discharge above the threshold of TH_{upper}; $Q_{Q>TH_{upper}}$ is the number of days above the threshold of TH_{upper}; $Q_{Q>TH_{lower;Flood}}$ is the number of flood days with discharge below the threshold of TH_{lower}; $Q_{Q>TH_{lower}}$ is the number of days below the threshold of TH_{lower}. The upper threshold TH_{upper}, lower threshold TH_{lower} and tolerance threshold Tol_{lower} are set 95% quantile, 50% quantile and 1% according to author's suggestion (Fischer et al., 2021).

3.6 Probability of Detection (POD)

In order to better compare the relationship between flood events (observed from DFO, MODIS and discharge) and flood days (derived from GRACE), we referred to the probability of detection (POD) index proposed by Yang et al. (2021) and made it more appropriate for our study.

$$POD = flood_{GRACE-based}/(flood_{observed} + flood_{miss}) \quad (7)$$

Where $flood_{GRACE-based}$ means flood events identified by GRACE, $flood_{observed}$ means DFO-recorded flood events, MODIS-derived flood events or discharge-derived flood events. If each flood events with a three- or five-day buffer could cover the GRACE-based flood days, we consider it a $flood_{GRACE-based}$ event.

4 Results

4.1 Flood days and Events Based on GRACE TWS and Precipitation Data

This study considers GRACE-based flood days obtained under the constraint of the 95th percentile of the entire time-series dataset. Figure 2 shows the global cumulative flood days and flood events from Apr. 1st, 2002—Aug. 31st, 2016, and Figure 3 shows the histograms of flood days and flood events corresponding to Figure 2. Although the number of flood days extracted above cannot accurately reflect how many flood events occurred, we can simplify the results such that a number of consecutive detected flood days, or the interval between two consecutive flood days, no more than 3 days or 5 days can be considered a flood event. The principle involves roughly calculating the spatial distribution of global flood event occurrences. Consistency was found between the global spatial distributions of flood events and flood days. We found that 99.8% of the grids around the world experienced fewer than 400 flood days except in Southeast Asian countries and countries at the junction of North and South America, which experienced more than 400 flood days from Apr. 1st, 2002—Aug. 31st, 2016. In addition,

the areas with the most flood days and events were mainly located in the tropics. Island countries, western Africa, India, the Himalayas, southern China, etc., were also prone to floods. From the perspective of the divided flood events, the numbers of grid cells with fewer than 100 events accounted for 96.15% (Figure 2 b), 97.11% (Figure 2 c) and 97.52% (Figure 2 d) of all grids.

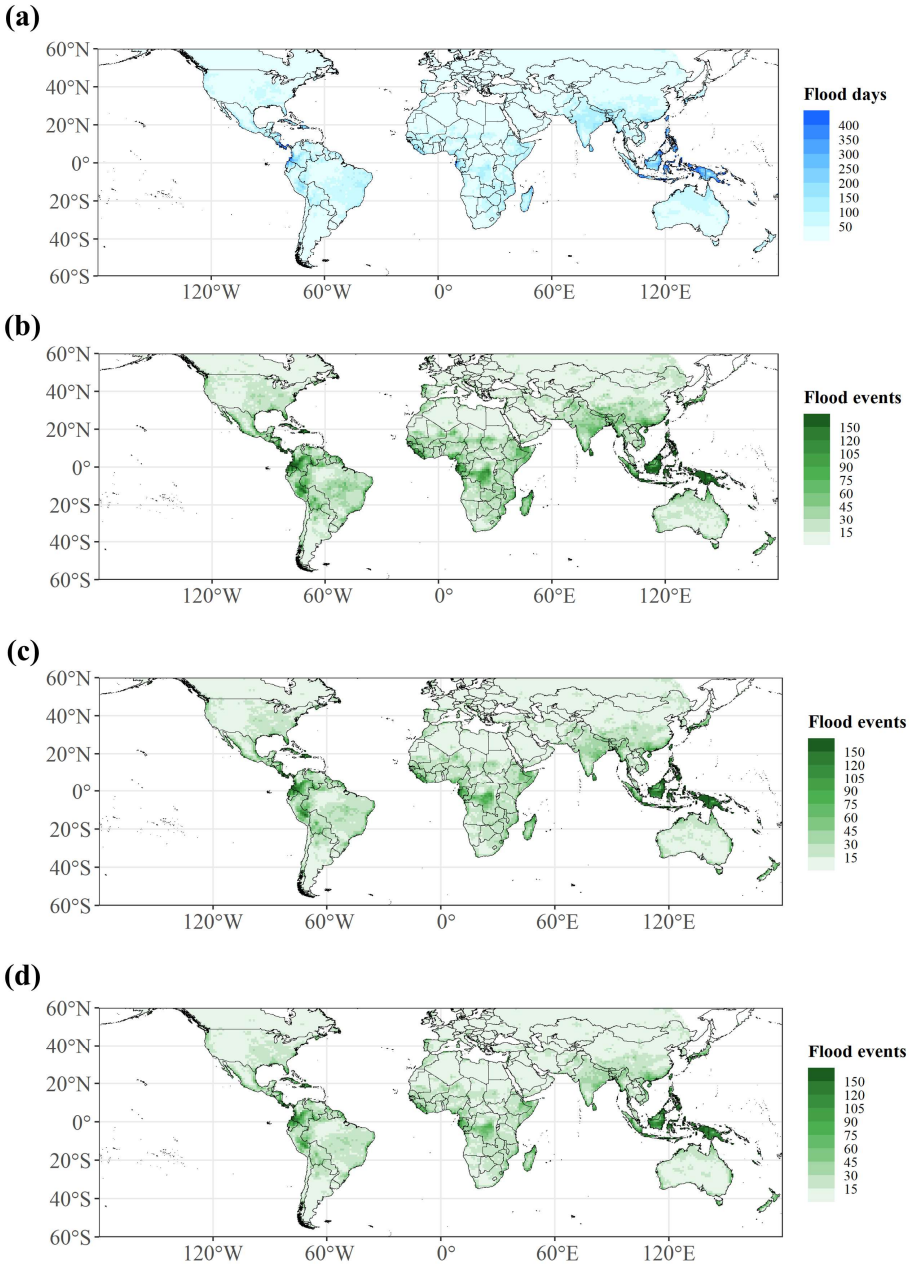

Figure 2 Spatial distribution of global floods, including (a) global flood days from Apr. 1st, 2002—Aug. 31st, 2016; (b) global flood events based on consecutive flood days; (c) global flood events based on the interval between two consecutive flood days not exceeding 3 days; and (d) global flood events based on the interval between two consecutive flood days not exceeding 5 days.

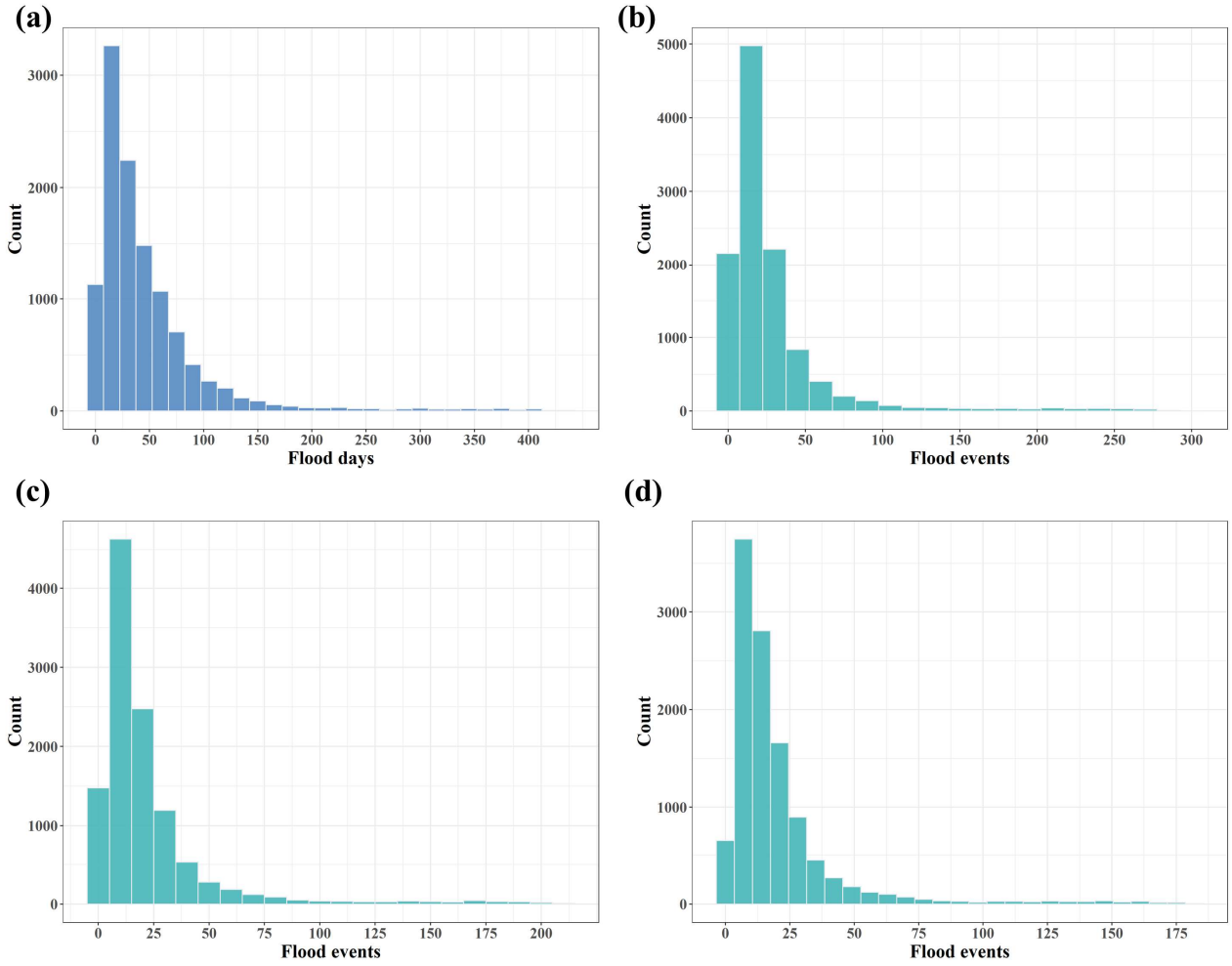

Figure 3 Histograms of cumulative flood days and flood events from Apr. 1st, 2002—Aug. 31st, 2016. (a) Histogram of global flood days from Apr. 1st, 2002—Aug. 31st, 2016; (b) histogram of global flood events based on consecutive detected flood days; (c) histogram of global flood events based on the interval between two consecutive flood days not exceeding 3 days; and (d) histogram of global flood events based on the interval between two consecutive flood days not exceeding 5 days.

We also calculated the average flood days in the same month in each year from 2002—2016 to identify seasonal characteristics. As shown in Figure 4, the global flood distribution reflected obvious seasonal characteristics, and differences between the Northern and Southern Hemispheres are clear. More flood days were identified in the Northern Hemisphere in summer (approximately June-September), while flood days in the Southern Hemisphere are concentrated from December-March.

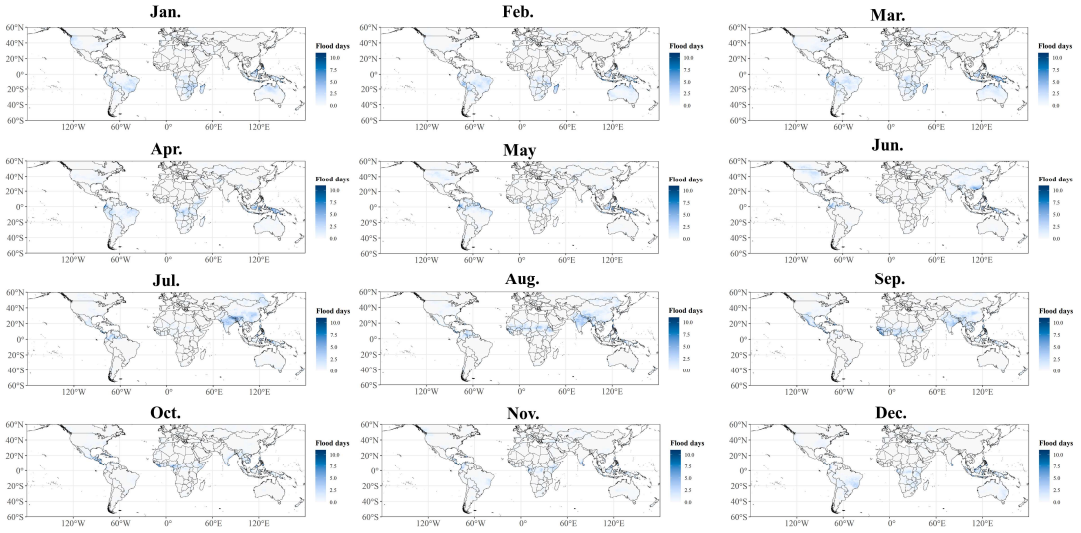

Figure 4 Average flood days in the same month of each year from 2002 to 2016.

4.2 Flood Days in Mountain Glacier Regions

We also analysed the distribution of flood days in the mountain glacier regions. We used global glacier outline data from the Randolph Glacier Inventory (RGI). This dataset can be used to estimate glacier volumes, rates of elevation change at regional and global scales, and the response of the cryosphere to climate forcing. The dataset is updated annually in shapefile format. We used it in this paper to locate global glaciers (Arendt et al., 2017).

In the range of 60°S—60°N, there are 10 glacier regions and 163 flood events recorded based on DFO database (Figure 5). 142 flood events were identified and 21 flood events were not detected, with a POD of 0.87. The capacity of flood detection is close to the global POD (0.81). The results showed that GRACE also has good potential in identifying precipitation-induced floods in glaciers regions. Of these 21 flood events, 4 flood events could not be identified due to missing months in GRACE data. 8 flood events had a maximum daily precipitation of less than 40 mm according to the DFO-recorded time period and spatial location (minimum: 8.44 mm, maximum: 36.56 mm) and GRACE could not identify the weaker signal. The remaining 9 flood events could not be identified due to GRACE itself failing to identify flood conditions.

We further selected the GRACE grid covering the glacier regions and analysed the characteristics of the extracted flood days. Figure 6 showed the 10 detailed glacier regions and the corresponding selected GRACE grids which covered the main glacier areas. Figure 7 showed the results of the extracted flood days related to the grid of each region. In general, the number of flood days in the glacier regions was relatively small, and mostly concentrated within 50 days from Apr. 1st, 2002 to Aug 31st, 2016, while the glaciers in the South Island of New Zealand and the glacier regions in the east of southern Asia were exceeded 100 days. The South Island of New Zealand where mountain glaciers are located experiences a hyper-maritime climate, and the west coast of the South Island receives the most precipitation, with annual precipitation >12 m (Anderson et al., 2010). Glacier regions in the east of south Asia are mainly located in the Himalayas, where normal climatic fluctuations become rather quick in the Himalayan sectors due to topography and the southwest Indian Ocean monsoon. It would occur cloud bursts, high winds, snowstorms, etc., further caused quick floods (Nandargi and Dhar, 2011).

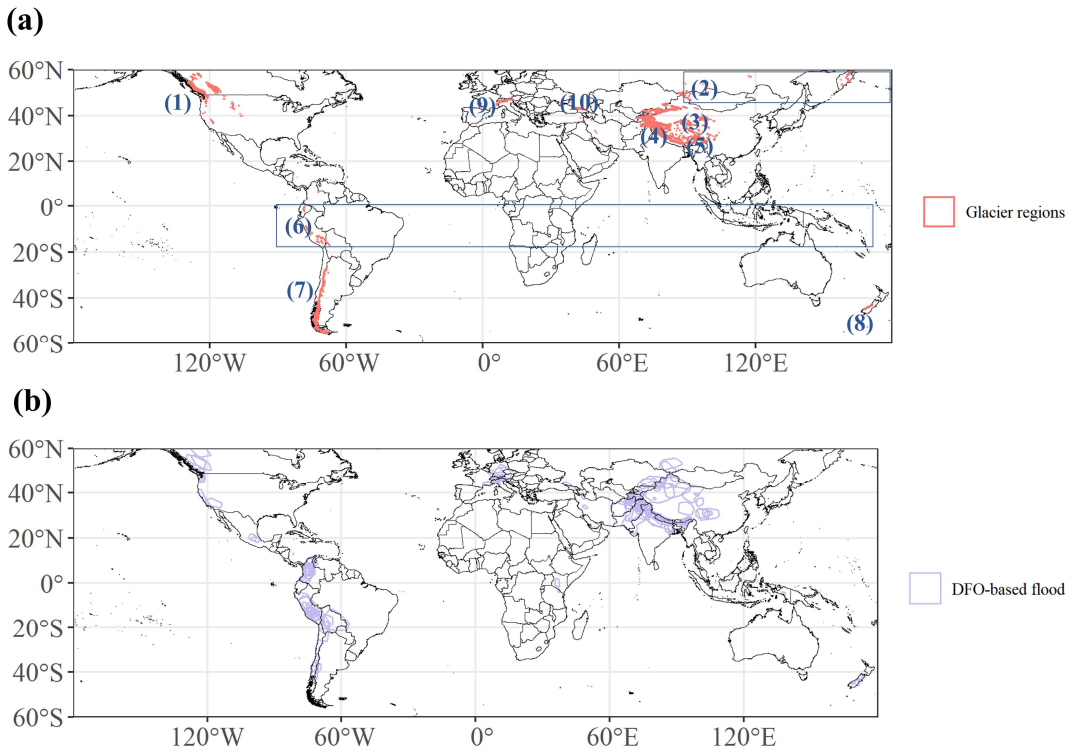

335

Figure 5 Global glacier distribution (a) and corresponding DFO-based flood events (b). (1) glacier regions in the western Canada and US; (2) glacier regions in north Asia; (3) glacier regions in central Asia; (4) glacier regions in the west of south Asia; (5) glacier regions in the east of south Asia; (6) glacier regions in the low latitudes; (7) glacier regions in the southern Andes; (8) glacier regions in the New Zealand; (9) glacier regions in the central Europe; (10) glacier regions in the middle east of Caucasus.

340

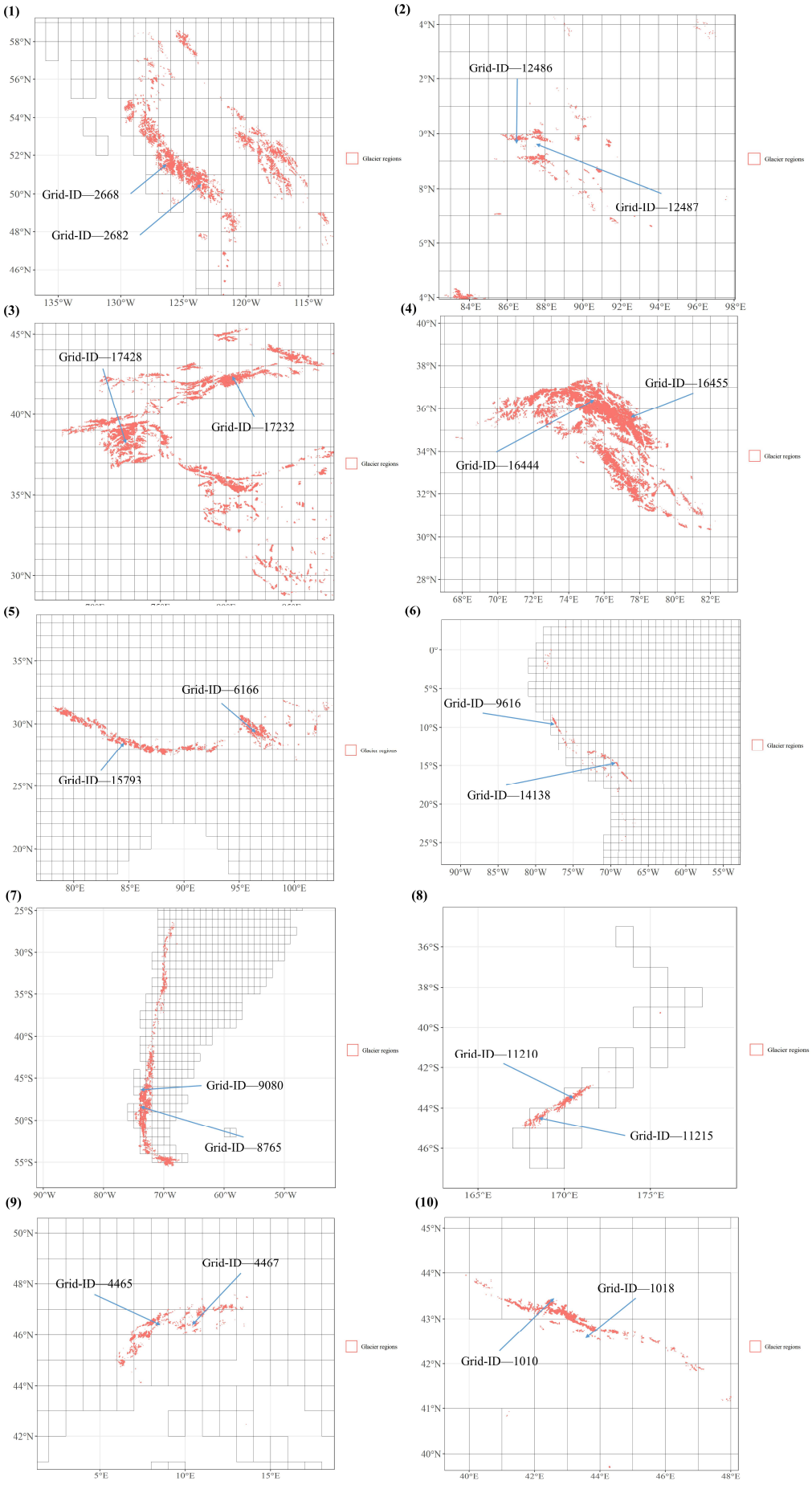

Figure 6 Ten glacier regions during the 60°S—60°N latitudes. two representative GRACE grid points in each region were selected to analyze the flood of the temporal detection. This was corresponding to the time series in Figure 7. (1) glacier regions in the western Canada and US; (2) glacier regions in north Asia; (3) glacier regions in central Asia; (4) glacier regions in the west of south Asia; (5)

glacier regions in the east of south Asia; (6) glacier regions in the low latitudes; (7) glacier regions in the southern Andes; (8) glacier regions in the New Zealand; (9) glacier regions in the central Europe; (10) glacier regions in the middle east of Caucasus.

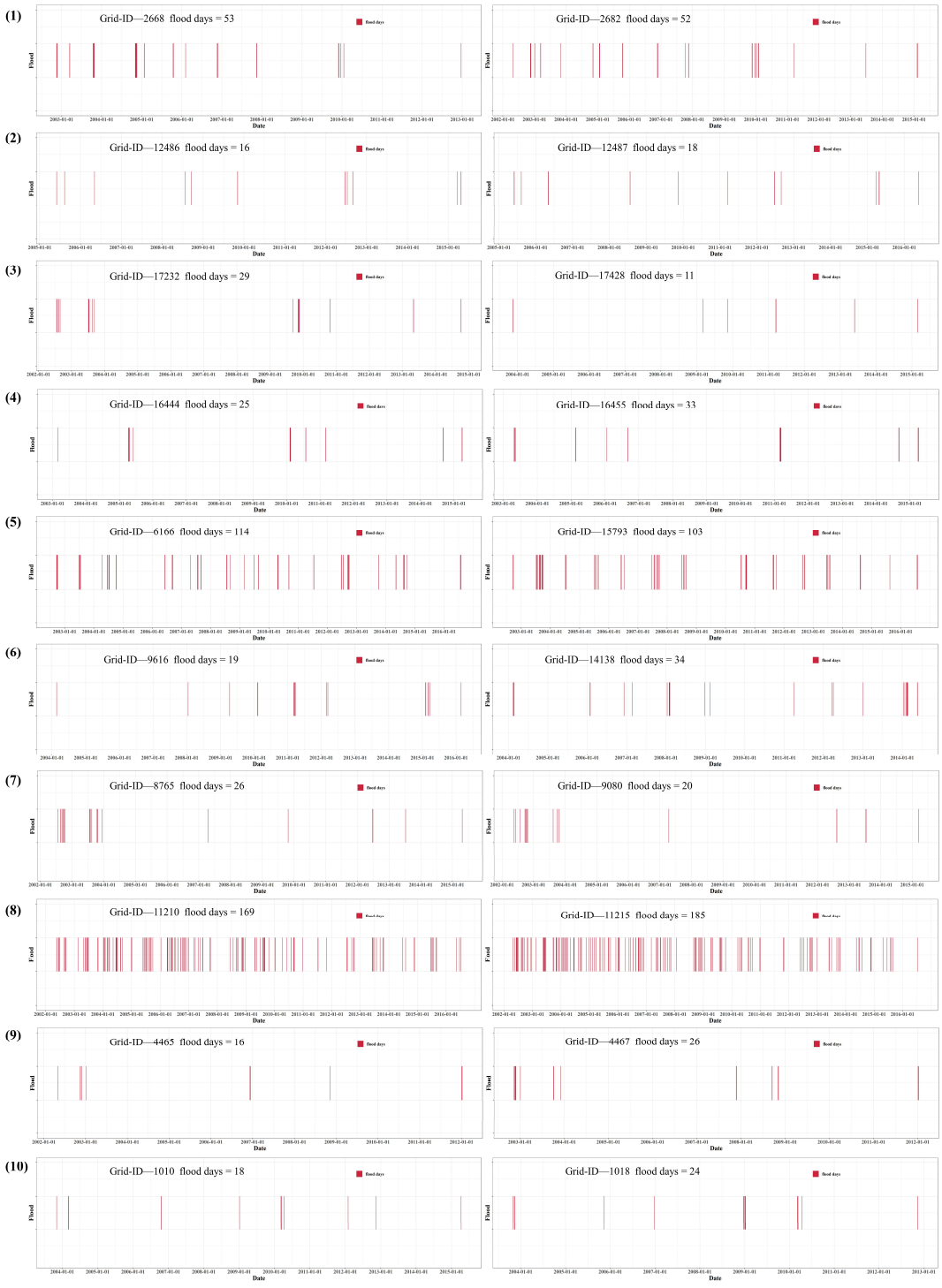

Figure 7 Flood detection results for different glacier regions (specific regions are consistent with Figure 6).

4.3 Validation with DFO and MODIS-derived Flood Data

Figure 8 shows the spatial distribution of 2,380 precipitation-type floods recorded by the global DFO from 60°S~ 60°N. Judging from the floods recorded by the DFO, floods have occurred in most parts of the world except in the Sahara Desert, the Great Victoria Desert and the northern part of North America.

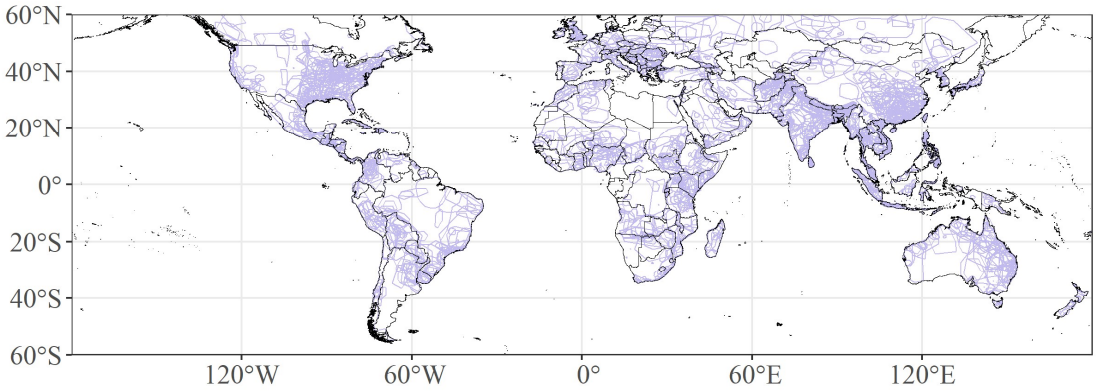

Figure 8 Spatial distribution of DFO-recorded flood events

In this study, the temporal length of the DFO database was compared with GRACE-based flood throughout the Apr. 1st, 2002—Aug. 31st, 2016 period. According to the database attributes, flood events caused by heavy precipitation were extracted as the validation dataset for this study. Given that the temporal and spatial DFO recording characteristics are approximate and considering the effect of advanced or delayed times on short-duration records, the start and end times of the DFO records were extended forward and backwards by three or five days, respectively, when being compared with the flood day results. Similarly, when the extent of the DFO polygon was less than 3 degrees, we appropriately built a buffer (3 degrees) to compensate for the positioning errors. Then, we detected every event in the DFO record to determine whether flood days could be identified from its temporal and spatial coverages.

Figure 9 shows the distribution of the number of flood events recorded by DFO on spatial 1-degree grids (the same as GRACE spatial resolution). It also shows that the eastern part of North America, the northern part of South America, the central and southern parts of Africa, western Europe, northern India and southern China are all areas with high-frequency flood events. Except for the archipelagic countries in Southeast Asia, the entire spatial distribution is consistent with our results.

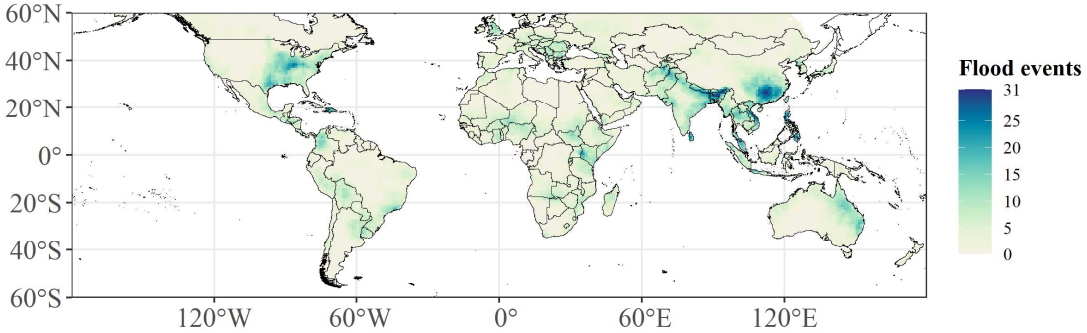

Figure 9 The frequency of flood events recorded by DFO distributed on 1-degree grids.

We compared the 2380 precipitation-type flood events recorded by the DFO one by one with the real flood extent extracted by Tellman et al. (2021) based on remote sensing images. Figure 10 shows part of the flood event comparison results derived based on GRACE, MODIS and DFO data. The dark blue polygons show the approximate flood ranges delineated by the DFO; red pixels are the flood inundation areas extracted based on MODIS data; and light blue regions show the flood days (≥1 day) extracted using GRACE TWS and extreme precipitation data during the period recorded by the DFO. MODIS-based

inundation extents were calculated according to the DFO time period and the union of DFO polygons and HydroSHEDS Basins Level 4 data (Tellman et al., 2021; Lehner et al., 2008; Lehner and Grill, 2013). We also used the DFO-recorded time series as a reference to filter flood days in each grid cell and obtained the spatial flood distributions in specific areas. The flood extents recorded by DFO are rough and time durations are sometimes long (much more than 1 month), which contained large uncertainties in spatial distribution and duration. Although MODIS resolution (1 km) is higher than that of GRACE TWS (1°, ~100km), only a limited amount of flooding can be identified by remote sensing images due to the influence of bad weather. The GRACE-based flood days we provided was only able to indicate the presence of flood events under the ~100km grid coverage, and specific detailed flood extents require further identification by high-resolution satellite remote sensing image. Therefore, we can see some differences among the spatial patterns of flood recorded by DFO, MODIS and GRACE. This study focuses on whether the flood events recorded by the DFO can be detected by GRACE, so as long as the number of flood days (≥1 day) extracted by GRACE could be found at the time and space specified by DFO, the effectiveness of the method could be demonstrated. Considering the results of 2380 events, 463 flood events were not detected, resulting in a detection rate of 81%. Among the undetected events, 85 events went undetected due to low precipitation (not the cases of extreme precipitation), while 69 went undetected due to the lack of GRACE data in certain months, resulting in the inability to obtain effective high-frequency signals. Among the remaining 309 undetected floods, the omission of 184 floods may have been caused by the fact that the maximum daily precipitation was less than 50 mm, causing GRACE to fail to identify a flood signal. The other 125 undetected flood events may have been caused by GRACE itself failing to identify flood conditions. To view the spatial distributions of precipitation-type floods and the corresponding situation obtained from flood inundation data extracted from GRACE and MODIS, please refer to the corresponding supplementary materials (https://doi.org/10.5281/zenodo.6831105 (Zhang et al., 2022a)).

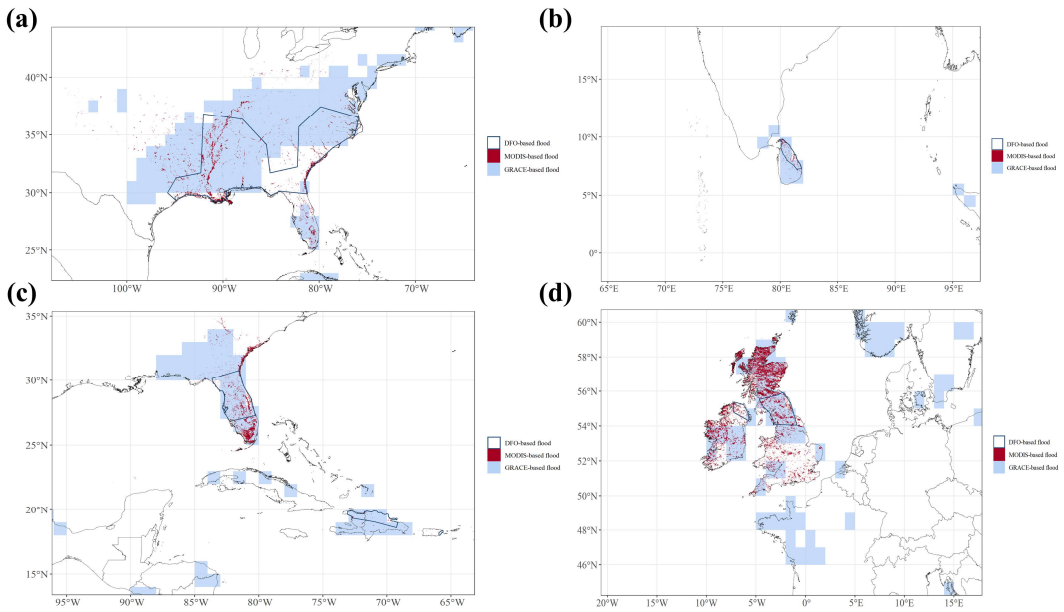

Figure 10 Flood inundation information recorded by the DFO (dark blue polygon), MODIS (red pixels) and GRACE (light blue). (a) The ID-2167 flood event that occurred from Feb. 22nd—Mar. 17th, 2003; (b) the ID-2601 flood event that occurred from Dec. 11th—Dec. 23rd, 2004; (c) the ID-2566 flood event that occurred from Sep. 15th—Oct. 1st, 2004; and (d) the ID-4319 flood event that occurred from Dec. 5th, 2015—Jan. 26th, 2016.

4.4 Further Validation with News Reports and Social Medias

We further selected some flood events through news reports and social medias (like Twitter, Weibo) to verify if there were some flood events that couldn't be identified by the DFO but can be identified by GRACE-based flood days. Figure 11 presented 9 flood events not recorded by the DFO, including floods that occurred in different time periods and areas such as

the eastern United States, northern and southern South America, Mozambique in Africa, France, India, China, Malaysia, Indonesia and Australia. The red boxes indicated the approximate location of the reported flood events. The blue areas were the GRACE-based flood days corresponding time duration and approximate location of flood events recorded by social media or news reports. We found that GRACE-based flood days could well identify these missing flood events, which also proved the effectiveness of using GRACE to identify large-scale flood events. Our data can be used as a good supplement to DFO data.

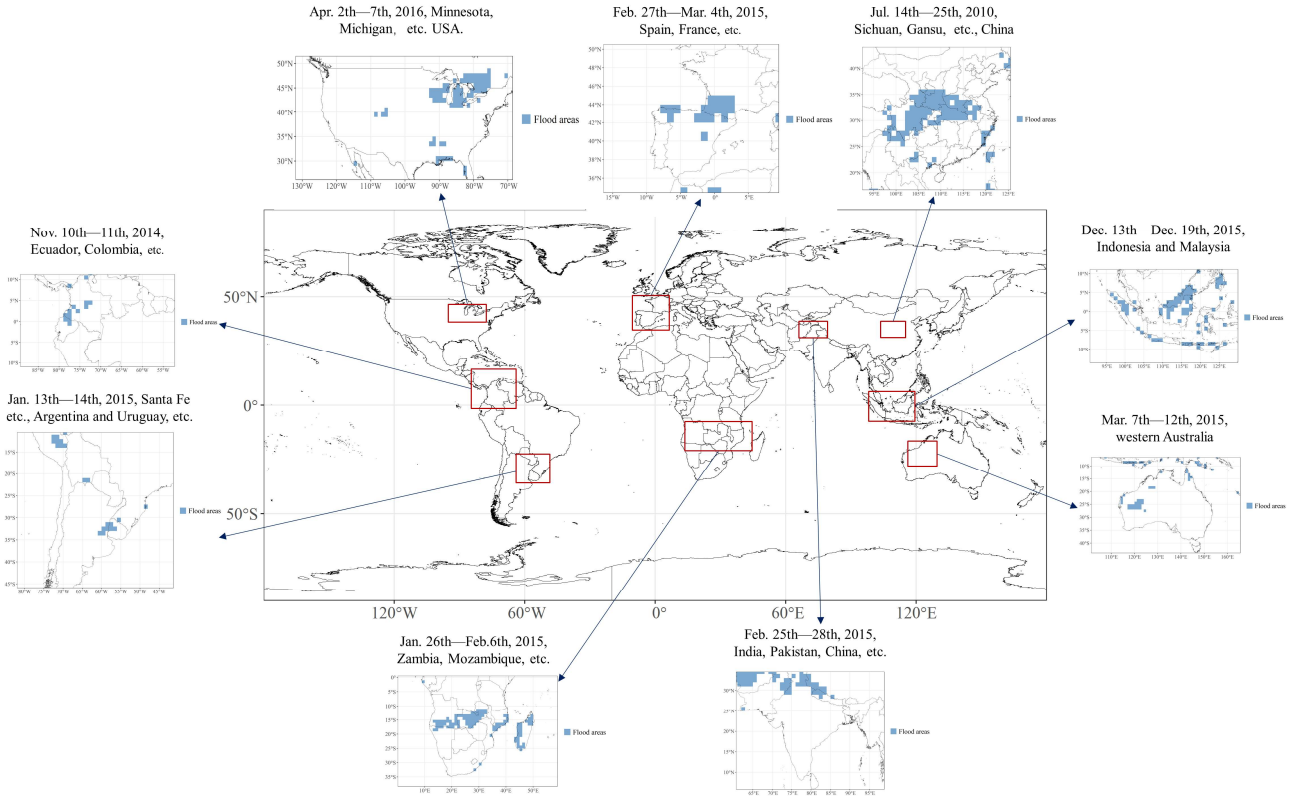

Figure 11 Validation of some flood events recorded by social media and news but not by the DFO.

4.5 Validation with Discharge Data

We also compared GRACE-based flood days with discharge data to assess our detection ability. We used the FloodR method of Fischer et al. (2021) to extract possible flood events from 3408 GRDC discharge data to serve as a basic reference standard when verifying the accuracy of the results extracted in this study. We focused on extreme precipitation-induced flood events and similarly constrained the results derived from the discharge data with extreme precipitation data. To ensure accuracy, we first selected the floods extracted from discharge stations with GFS greater than 0.5 for comparison. Due to discharge reflects the amount of water integrated over its entire contributing basin and contributing time (Yang et al., 2019), we combined the flood events obtained from each discharge station in time series to describe the flood events in the 261 watershed (HydroSHEDS Basins Level 4 (Lehner and Grill, 2013; Lehner et al., 2008)). Flood events in the same watershed were merged according to whether there was an intersection in the time series. The accuracy index used for comparison in this study is the probability of detection (POD) (Yang et al., 2021), i.e., whether each flood event in the river basin contained the GRACE-based flood days. Although flood events derived from discharge cannot guarantee that the surrounding land will experience flooding, it provides us a reference to support the reliability of the time series verification process.

Figure 12 showed the global distribution of discharge location and the goodness of flood separation. The data distributions in North America, South America, Europe and south-eastern Australia were relatively dense, while data were seriously missing

in central, northern and eastern Asia. The areas with higher GFS were located in the eastern part of the United States and central Europe, and the stations recorded in these areas were relatively complete. The discharge stations with GFS above 0.5 accounted for 73.49%. Figure 13 showed the flood events in the level-4 river basins. We find that most flood events reflected by the discharge data are mainly located in the eastern and western United States, central South America, eastern Europe and New Zealand.

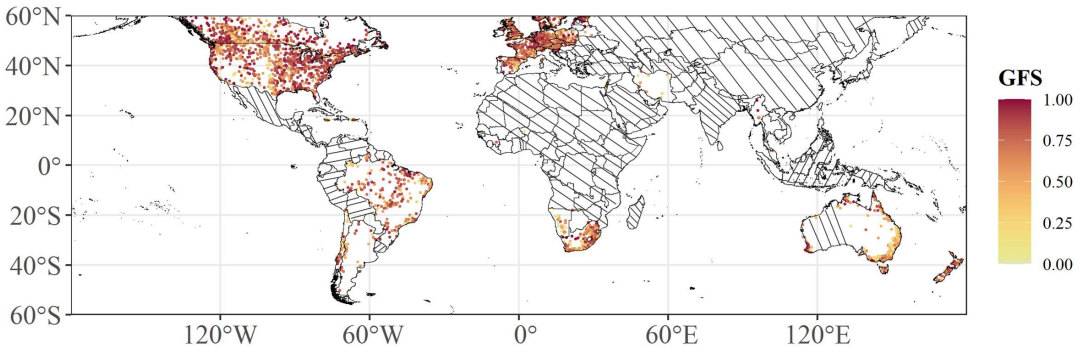

Figure 12 GFS of 3408 discharge sites around the world. The slant line means no data.

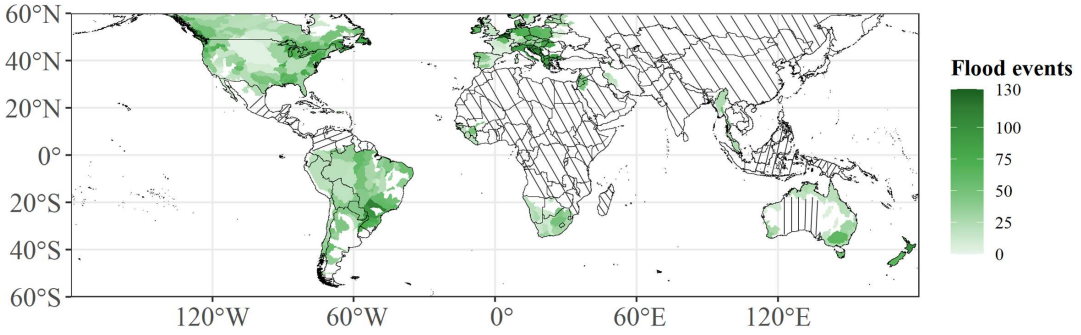

Figure 13 Flood events distribution in the Level-4 basins. The slant line means no data.

The POD calculation results are shown in Figure 14. The darker the colour is, the higher the corresponding flood detection accuracy is. We found that the overall accuracy performed well; the detection accuracies obtained for the central and eastern parts of the United States, western South America, southern Africa and around Australia are relatively high. Figure 15 showed the histogram of 261 watersheds of level-4 basins and the percentage of river basins with POD values greater than or equal to 0.5 reached 62 %. This finding showed that our extracted flood days also reflected relatively high accuracies in comparison with flood events at river basins.

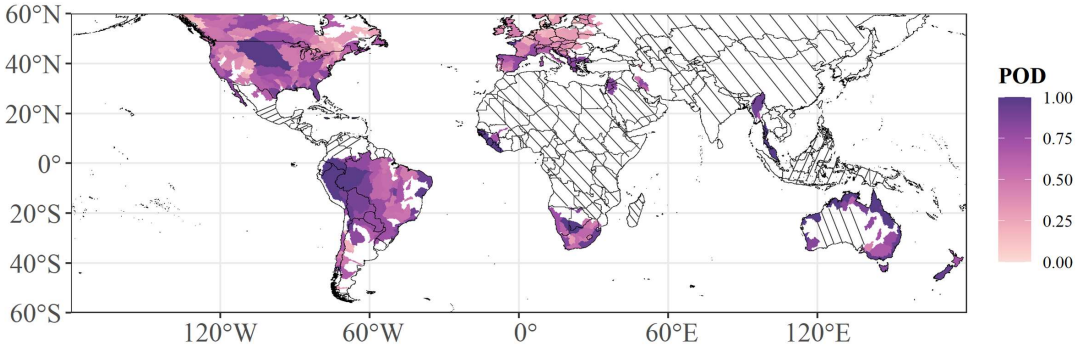

Figure 14 POD values in the Level-4 basins. The slant line means no data.

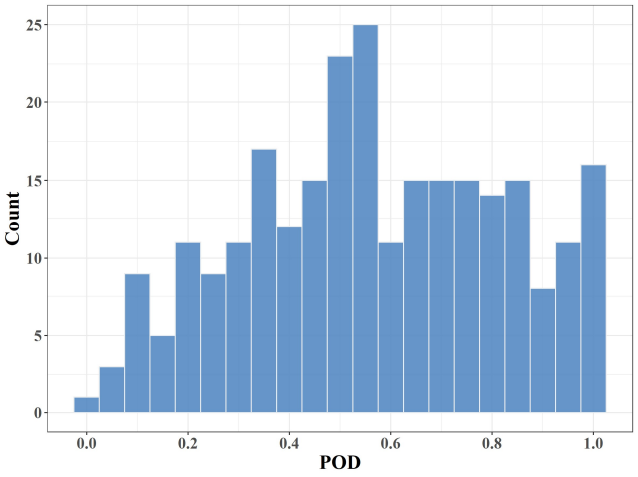

Figure 15 The histogram of POD in 261 river basins.

We listed flood detection performance compared with DFO, MODIS and discharge respectively in the Table 1. GRACE was able to detect 81% of flood events recorded by DFO and 87% of flood events recorded by MODIS. If we summed all flood events from 261 river basins, GRACE-based flood days could identify 53% flood events derived from discharges. The percentage of river basins with POD values greater than or equal to 0.5 reached 62%.

Table 1 Flood detection performance compared with DFO, MODIS and discharge data

	DFO (number of flood events)	MODIS (number of flood events)	Discharge (number of flood events)	Discharge (number of river basins)
Total	2380	807	10472	261
Detection	1917	703	5597	156 (POD>=0.5)
Percent	81%	87%	53%	62%

4.6 Uncertainty Analysis

The uncertainty analysis performed in this study mainly focused on the selection of the extreme precipitation threshold. The most common method for determining the extreme precipitation threshold is to use the quantile of the analysed time series, considering either the quantile of the entire time series (QETS) data or the quantile of wet days with daily precipitation greater than 1 mm (QWDTS). This study compared the different PODs under different quantile threshold scenario when comparing with DFO database. We selected the 90th, 95th and 99th quantiles for the two methods described above. Figure 16 shows that the selection of different thresholds in the two extreme precipitation scenarios influenced the flood extraction accuracy of POD with contributions ranging from 72.4% to 81.4%. This shows that the selected thresholds can affect the detection rate of approximately 9% (approximately 214) of flood events. We also provide the 6 products derived based on these two constraints for further analysis and use by researchers.

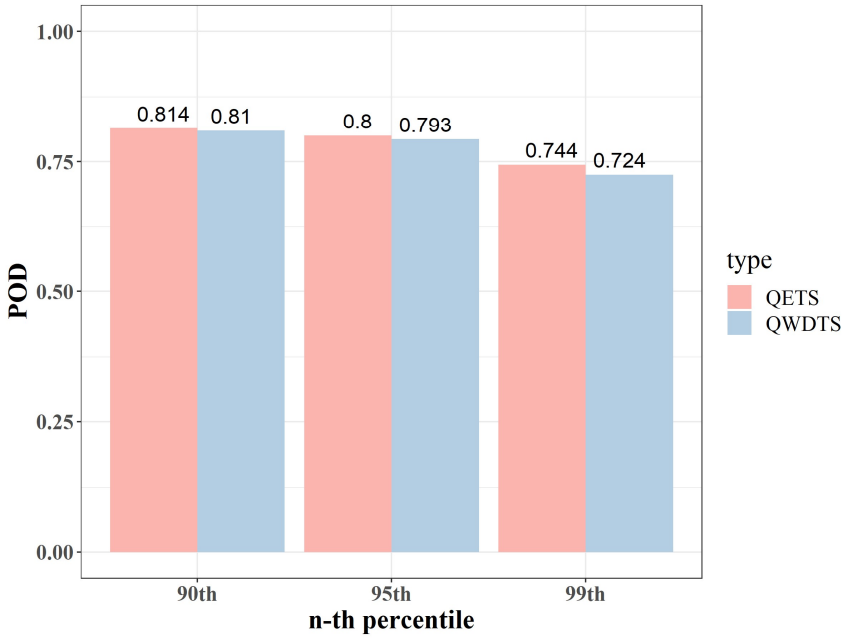

Figure 16 Influence of the selected threshold and extreme precipitation standard on the POD

5 Data Usage Instructions

The data obtained herein are provided using the polygon shapefile (SHP file) format. A separate file is provided for each day, and each file represents the global flood day distribution. The spatial resolution is 1°, covering range of 60°S—60°N from Apr. 1st, 2002, to Aug. 31st, 2016. The SHP files have two fields, namely, "ID" and "Value"; "ID" represents the index number of the 1° grid, and "Value" is a binary variable (with a value of 0 or 1) indicating whether a flood occurred on the specific day. This flood day product can be used to analyse the spatial distributions of historical flood days within 60° north-south latitude and extract specific flood events in combination with historical data from observation sites. At the same time, the products are obtained based on observed data and can be used to verify flood model results. Considering that the El Niño-Southern Oscillation affects both drought and flood events in different parts of the world, these data can be used to further analyse the impacts of the El Niño-Southern Oscillation on flood days around the world.

6 Data availability

The flood day product produced in this study can be obtained from https://doi.org/10.5281/zenodo.6831384 (Zhang et al., 2022b).

7 Conclusion and Discussion

This study successfully extracted global flood days using GRACE TWS and extreme precipitation data between 60°S and 60°N from Apr. 1st, 2002 to Aug. 31st, 2016. The results were compared in time and space with the flood events recorded by the DFO, MODIS and discharge. It showed that GRACE-based flood events could identify 81% of the flood events recorded by the DFO and 87% flood events derived from MODIS. To further verify the reliability of our GRACE-based flood products, we compared them with the flood events extracted from global GRDC discharge data, and the probability of detection greater than or equal to 0.5 reached 62% at river basin scale. Moreover, we selected representative flood events not recorded by the DFO but recorded in social media and news in different regions of the world as verification examples. These results also showed that our GRACE-based flood days could identify and supplement flood events not recorded by DFO. The value of our product is mainly reflected in the following aspects. First, the GRACE-based flood days own wide coverage (covering

between 60°S and 60°N). Second, it is continuous in time and space and the number of flood days in different areas or in different research time scales can be calculated according to research needs, which makes up for the lack of flood events due to weather condition for MODIS and records missing for DFO. Third, it provides not only important data support for the spatiotemporal distributions and attributions of global flood events, but also a reference for large-scale quasi-real-time flood event monitoring with the development of GRACE-FO and the quality improvement of GRACE daily data.

We also acknowledge that there are some limitations to these data. First, we used extreme precipitation to constrain the data, and the detection ability of some small floods was thus insufficient. Second, considering the regional differences of precipitation at GRACE resolution level, the maximum precipitation under the GRACE grid can retain the signal of extreme precipitation to the greatest extent. We have also tried to take the mean value of the precipitation covered by GRACE grid, but this led to many missing flood events. Third, the high frequency signals of GRACE TWS may loss some flood events as demonstrated before. Although FPI can supplement some flood events that were not identified by high-frequency signals, it can not guarantee that all flood events lost due to high-frequency signals could be supplemented. Fourth, the GRACE-based days are affected by ocean signals around island countries due to the coarse data resolution, and researchers should be careful when using these data in such areas. Fifth, we were not able to compute the false detection of flood events. Due to the difficulty in observation, a complete and correct global record of floods is unavailable. This also highlights the importance of this study which tries to provide a new approach for detecting global flood events. Although we cannot calculate the false alarm rate, we can calculate the corresponding detection rate (i.e. POD) for the existing recorded floods and selected larger flood events recorded by news reports or social medias (not recorded by DFO) for further comparison. Sixth, we cannot correctly separate specific flood events from GRACE-based flood days and separate false flood detection from non-recorded flood cases, which are also direction that needs further study in the future.

Acknowledgements

The research in this article was supported by the National Natural Science Foundation of China [grant number 41771538]. The financial support is highly appreciated. We also thank the data support of the GRACE daily solution from the Institute of Geodesy, Graz University of Technology.

Conflicts of Interest: The authors declare that they have no conflicts of interest.

Author Contributions

Conceptualization, K. L., J. Z., and M. W.; Methodology, J. Z., K. L., and M. W.; Validation, J. Z. and K. L.; Formal Analysis, J. Z. and K. L.; Investigation, J. Z., K. L., and M. W.; Resources, J. Z.; Data Curation, J. Z.; Writing-Original Draft Preparation, J. Z.; Writing-Review & Editing, K. L.; Visualization, J. Z; Supervision, K. L.; Project Administration, K. L.; Funding Acquisition, K. L. All authors have read and agreed to the published version of the manuscript.

References

Aggarwal, Charu C: Outlier ensembles: position paper, ACM SIGKDD Explorations Newsletter, 14, 49-58, 2013.

Anderson, Brian, Mackintosh, Andrew, Stumm, Dorothea, George, Laurel, Kerr, Tim, Winter-Billington, Alexandra, and Fitzsimons, Sean: Climate sensitivity of a high-precipitation glacier in New Zealand, Journal of Glaciology, 56, 114-128, 2010.

Arendt, A, Bliss, A, Bolch, T, Cogley, JG, Gardner, A, Hagen, J-O, Hock, R, Huss, M, Kaser, G, and Kienholz, C: Randolph Glacier inventory–A dataset of Global glacier outlines: Version 6.0: Technical report, Global land ice measurements from space, 2017.

Bergmann-Wolf, Inga, Forootan, Ehsan, Klemann, Volker, Kusche, Jürgen, and Dobslaw, Henryk:

Updating ESA's Earth System Model for Gravity Mission Simulation Studies: 3. A Realistically Perturbed Non-Tidal Atmosphere and Ocean De-Aliasing Model, 2015.
Brakenridge, G Robert: Global Active Archive of Large Flood Events. Dartmouth Flood Observatory, University of Colorado, USA. http://floodobservatory.colorado.edu/ Archives/ (Accessed Jan.1, 2022). 2022.
Cazenave, Anny and Chen, Jianli: Time-variable gravity from space and present-day mass redistribution in theEarth system, Earth and Planetary Science Letters, 298, 263-274, 2010.
Chandola, Varun, Banerjee, Arindam, and Kumar, Vipin: Anomaly detection: A survey, ACM computing surveys (CSUR), 41, 1-58, 2009.
Clark, Elyse V and Zipper, Carl E: Vegetation influences near-surface hydrological characteristics on a surface coal mine in eastern USA, Catena, 139, 241-249, 2016.
de Bruijn, Jens A, de Moel, Hans, Jongman, Brenden, de Ruiter, Marleen C, Wagemaker, Jurjen, and Aerts, Jeroen CJH: A global database of historic and real-time flood events based on social media, Scientific data, 6, 1-12, 2019.
Dill, Robert, Thomas, Maik, and Walter, C: Hydrological induced Earth rotation variations from standalone and dynamically coupled simulations, Proceedings of the Journées,
EM-DAT, CRED: Centre for research on the epidemiology of disasters, EM Dat The international Disaster Database https://public.emdat.be/ 2014.
Fischer, Svenja, Schumann, Andreas, and Bühler, Philipp: A statistics-based automated flood event separation, Journal of Hydrology X, 10, 100070, 2021.
Gorelick, Noel, Hancher, Matt, Dixon, Mike, Ilyushchenko, Simon, Thau, David, and Moore, Rebecca: Google Earth Engine: Planetary-scale geospatial analysis for everyone, Remote sensing of Environment, 202, 18-27, 2017.
Gouweleeuw, Ben T, Kvas, Andreas, Gruber, Christian, Gain, Animesh K, Mayer-Gürr, Thorsten, Flechtner, Frank, and Güntner, Andreas: Daily GRACE gravity field solutions track major flood events in the Ganges–Brahmaputra Delta, Hydrology and Earth System Sciences, 22, 2867-2880, 2018.
Gupta, Diksha and Dhanya, CT: The potential of GRACE in assessing the flood potential of Peninsular Indian River basins, International Journal of Remote Sensing, 41, 9009-9038, 2020.
Hagen, Emlyn, Shroder Jr, JF, Lu, XX, and Teufert, John F: Reverse engineered flood hazard mapping in Afghanistan: A parsimonious flood map model for developing countries, Quaternary International, 226, 82-91, 2010.
Hostache, Renaud, Chini, Marco, Giustarini, Laura, Neal, Jeffrey, Kavetski, Dmitri, Wood, Melissa, Corato, Giovanni, Pelich, Ramona - Maria, and Matgen, Patrick: Near - real - time assimilation of SAR - derived flood maps for improving flood forecasts, Water Resources Research, 54, 5516-5535, 2018.
Huffman, George J, Bolvin, David T, Nelkin, Eric J, and Tan, Jackson: Integrated Multi-satellitE Retrievals for GPM (IMERG) technical documentation, Nasa/Gsfc Code, 612, 2019, 2015.
Huggel, Christian, Raissig, Annik, Rohrer, Mario, Romero, Gilberto, Diaz, A, and Salzmann, Nadine: How useful and reliable are disaster databases in the context of climate and global change? A comparative case study analysis in Peru, Natural hazards and earth system sciences, 15, 475-485, 2015.
Idowu, Dorcas and Zhou, Wendy: Performance evaluation of a potential component of an early flood warning system—A case study of the 2012 flood, Lower Niger River Basin, Nigeria, Remote Sensing, 11, 1970, 2019.
Kron, Wolfgang, Steuer, Markus, Löw, Petra, and Wirtz, Angelika: How to deal properly with a natural catastrophe database–analysis of flood losses, Natural Hazards and Earth System Sciences, 12, 535-550, 2012.
Kussul, Nataliia, Shelestov, Andrii, and Skakun, Sergii: Flood monitoring from SAR data, in: Use of satellite and in-situ data to improve sustainability, Springer, 19-29, 2011.
Kvas, Andreas, Behzadpour, Saniya, Ellmer, Matthias, Klinger, Beate, Strasser, Sebastian, Zehentner, Norbert, and Mayer - Gürr, Torsten: ITSG - Grace2018: Overview and evaluation of a new GRACE - only gravity field time series, Journal of Geophysical Research: Solid Earth, 124, 9332-9344, 2019.
Lehner, Bernhard and Grill, Günther: Global river hydrography and network routing: baseline data and new approaches to study the world's large river systems, Hydrological Processes, 27, 2171-2186, 2013.

Lehner, Bernhard, Verdin, Kristine, and Jarvis, Andy: New global hydrography derived from spaceborne elevation data, Eos, Transactions American Geophysical Union, 89, 93-94, 2008.
Manavalan, Ramanuja: SAR image analysis techniques for flood area mapping-literature survey, Earth Science Informatics, 10, 1-14, 2017.
Mayer-Gürr, Torsten, Behzadpour, Saniya, Kvas, Andreas, Ellmer, Matthias, Klinger, Beate, Strasser, Sebastian, and Zehentner, Norbert: ITSG-Grace2018 - Monthly, Daily and Static Gravity Field Solutions from GRACE. GFZ Data Services. https://doi.org/10.5880/ICGEM.2018.003, 2018.
Molodtsova, Tatiana, Molodtsov, Sergey, Kirilenko, Andrei, Zhang, Xiaodong, and VanLooy, Jeffrey: Evaluating flood potential with GRACE in the United States, Natural Hazards and Earth System Sciences, 16, 1011-1018, 2016.
Moriyama, Kana, Sasaki, Daisuke, and Ono, Yuichi: Comparison of global databases for disaster loss and damage data, Journal of Disaster Research, 13, 1007-1014, 2018.
Myhre, Gunnar, Alterskjær, Kari, Stjern, Camilla Weum, Hodnebrog, Øivind, Marelle, Louis, Samset, Bjørn Hallvard, Sillmann, Jana, Schaller, Nathalie, Fischer, Erich, and Schulz, Michael: Frequency of extreme precipitation increases extensively with event rareness under global warming, Scientific reports, 9, 1-10, 2019.
Nandargi, S and Dhar, ON: Extreme rainfall events over the Himalayas between 1871 and 2007, Hydrological Sciences Journal, 56, 930-945, 2011.
Pendergrass, Angeline G: What precipitation is extreme?, Science, 360, 1072-1073, 2018.
Rättich, Michaela, Martinis, Sandro, and Wieland, Marc: Automatic flood duration estimation based on multi-sensor satellite data, Remote Sensing, 12, 643, 2020.
Re, Swiss: Sigma: Insurance research.available at http://www.swissre.com/sigma/ (last access: 18 Jun. 2022), 2022.
Reager, John T and Famiglietti, James S: Global terrestrial water storage capacity and flood potential using GRACE, Geophysical research letters, 36, 2009.
Reager, John T, Thomas, Brian F, and Famiglietti, James S: River basin flood potential inferred using GRACE gravity observations at several months lead time, Nature Geoscience, 7, 588-592, 2014.
Robert, Cleveland, William, C, and Irma, Terpenning: STL: A seasonal-trend decomposition procedure based on loess, Journal of official statistics, 6, 3-73, 1990.
Rosner, Bernard: Percentage points for a generalized ESD many-outlier procedure, Technometrics, 25, 165-172, 1983.
Saghafian, Bahram, Golian, Saeed, and Ghasemi, Alireza: Flood frequency analysis based on simulated peak discharges, Natural Hazards, 71, 403-417, 2014.
Schinko, Thomas, Mechler, Reinhard, and Hochrainer-Stigler, Stefan: A methodological framework to operationalize climate risk management: managing sovereign climate-related extreme event risk in Austria, Mitigation and Adaptation Strategies for Global Change, 22, 1063-1086, 2017.
Shi, Xinyan, Chen, Jie, Gu, Lei, Xu, Chong-Yu, Chen, Hua, and Zhang, Liping: Impacts and socioeconomic exposures of global extreme precipitation events in 1.5 and 2.0° C warmer climates, Science of The Total Environment, 766, 142665, 2021.
Tellman, B, Sullivan, JA, Kuhn, C, Kettner, AJ, Doyle, CS, Brakenridge, GR, Erickson, TA, and Slayback, DA: Satellite imaging reveals increased proportion of population exposed to floods, Nature, 596, 80-86, 2021.
Tong, Xiaohua, Luo, Xin, Liu, Shuguang, Xie, Huan, Chao, Wei, Liu, Shuang, Liu, Shijie, Makhinov, AN, Makhinova, AF, and Jiang, Yuying: An approach for flood monitoring by the combined use of Landsat 8 optical imagery and COSMO-SkyMed radar imagery, ISPRS journal of photogrammetry and remote sensing, 136, 144-153, 2018.
Vallis, Owen, Hochenbaum, Jordan, and Kejariwal, Arun: A Novel Technique for {Long-Term} Anomaly Detection in the Cloud, 6th USENIX workshop on hot topics in cloud computing (HotCloud 14),
Wahr, John, Molenaar, Mery, and Bryan, Frank: Time variability of the Earth's gravity field: Hydrological and oceanic effects and their possible detection using GRACE, Journal of Geophysical Research: Solid Earth, 103, 30205-30229, 1998.
Winsemius, HC, Van Beek, LPH, Jongman, B, Ward, PJ, and Bouwman, A: A framework for global river flood risk assessments, Hydrology and Earth System Sciences, 17, 1871-1892, 2013.

Wu, Huan, Kimball, John S, Mantua, Nate, and Stanford, Jack: Automated upscaling of river networks for macroscale hydrological modeling, Water Resources Research, 47, 2011.
Wu, Huan, Adler, Robert F, Hong, Yang, Tian, Yudong, and Policelli, Fritz: Evaluation of global flood detection using satellite-based rainfall and a hydrologic model, Journal of Hydrometeorology, 13, 1268-1284, 2012a.
Wu, Huan, Adler, Robert F, Tian, Yudong, Huffman, George J, Li, Hongyi, and Wang, JianJian: Real‐time global flood estimation using satellite‐based precipitation and a coupled land surface and routing model, Water Resources Research, 50, 2693-2717, 2014.
Wu, Huan, Kimball, John S, Li, Hongyi, Huang, Maoyi, Leung, L Ruby, and Adler, Robert F: A new global river network database for macroscale hydrologic modeling, Water resources research, 48, 2012b.
Xiong, Jinghua, Wang, Zhaoli, Guo, Shenglian, Wu, Xushu, Yin, Jiabo, Wang, Jun, Lai, Chengguang, and Gong, Qiangjun: High effectiveness of GRACE data in daily-scale flood modeling: case study in the Xijiang River Basin, China, Natural Hazards, 1-20, 2022.
Yang, Yuan, Lin, Peirong, Fisher, Colby K, Turmon, Michael, Hobbs, Jonathan, Emery, Charlotte M, Reager, John T, David, Cédric H, Lu, Hui, and Yang, Kun: Enhancing SWOT discharge assimilation through spatiotemporal correlations, Remote Sensing of Environment, 234, 111450, 2019.
Yang, Yuan, Pan, Ming, Lin, Peirong, Beck, Hylke E, Zeng, Zhenzhong, Yamazaki, Dai, David, Cédric H, Lu, Hui, Yang, Kun, and Hong, Yang: Global Reach-Level 3-Hourly River Flood Reanalysis (1980–2019), Bulletin of the American Meteorological Society, 102, E2086-E2105, 2021.
Zhang, Jianxin, Liu, Kai , and Wang, Ming: Flood detection using GRACE Terrestrial Water Storage and Extreme Precipitation (1.0.0). Zenodo. https://doi.org/10.5281/zenodo.6831105, 2022a.
Zhang, jianxin, Liu, Kai, and Wang, Ming: Flood Detection Using GRACE Terrestrial Water Storage and Extreme Precipitation (1.0.0) [Data set]. Zenodo. https://doi.org/10.5281/zenodo.6831384, 2022b.